Increased brain uptake of targeted nanoparticles by adding an acid-cleavable linkage between transferrin and the nanoparticle core

Andrew J. Clark and Mark E. Davis[1]

Division of Chemistry and Chemical Engineering, California Institute of Technology, Pasadena, CA 91125

Contributed by Mark E. Davis, August 27, 2015 (sent for review August 13, 2015)

Most therapeutic agents are excluded from entering the central nervous system by the blood–brain barrier (BBB). Receptor mediated transcytosis (RMT) is a common mechanism used by proteins, including transferrin (Tf), to traverse the BBB. Here, we prepared Tf-containing, 80-nm gold nanoparticles with an acid-cleavable linkage between the Tf and the nanoparticle core to facilitate nanoparticle RMT across the BBB. These nanoparticles are designed to bind to Tf receptors (TfRs) with high avidity on the blood side of the BBB, but separate from their multidentate Tf–TfR interactions upon acidification during the transcytosis process to allow release of the nanoparticle into the brain. These targeted nanoparticles show increased ability to cross an in vitro model of the BBB and, most important, enter the brain parenchyma of mice in greater amounts in vivo after systemic administration compared with similar high-avidity nanoparticles containing noncleavable Tf. In addition, we investigated this design with nanoparticles containing high-affinity antibodies (Abs) to TfR. With the Abs, the addition of the acid-cleavable linkage provided no improvement to in vivo brain uptake for Ab-containing nanoparticles, and overall brain uptake was decreased for all Ab-containing nanoparticles compared with Tf-containing ones. These results are consistent with recent reports of high-affinity anti-TfR Abs trafficking to the lysosome within BBB endothelium. In contrast, high-avidity, Tf-containing nanoparticles with the acid-cleavable linkage avoid major endothelium retention by shedding surface Tf during their transcytosis.

blood–brain barrier | transcytosis | therapeutic delivery | systemic administration | in vivo

The inability of drugs to cross the blood–brain barrier (BBB) is one of the major impairments to developing treatments for neurological diseases. This highly restrictive, physiologic barrier excludes 98% of small-molecule drugs and ∼100% of large-molecule drugs from reaching the central nervous system (CNS) from blood circulation (1). Many methods to bypass the BBB have been investigated, such as transient disruption of the BBB, inhibition of efflux pumps, or transport using endogenous transcytosis systems, including receptor-mediated transcytosis (2–4).

Transferrin receptor (TfR) has been one of the primary targets investigated for receptor-mediated transcytosis across the BBB because of its high expression on BBB endothelium (5). Anti-TfR antibody–drug conjugates have received the most attention because of their ability to bind TfR with high affinity without interfering with endogenous transferrin (Tf) (6–8). Despite the perceived potential of anti-TfR antibody–drug conjugates, a BBB-permeable drug using this approach has yet to reach the clinic. Yu et al. showed that anti-TfR Abs enter the brain in greater numbers when their affinity to TfR is reduced (9). Follow-up work from the same group showed that high-affinity, bispecific anti-TfR Abs preferentially trafficked to the lysosome within BBB endothelium, rather than transcytosing, whereas low-affinity Abs did not (10). A similar effect was seen with a divalent anti-TfR Ab, which entered the lysosome in significantly greater amounts than the monovalent variant (11).

Recently, our group demonstrated that Tf-containing, 80-nm gold nanoparticles (AuNP) with near-neutral zeta potentials are capable of accessing the brain parenchyma from the blood when their avidity to TfR is appropriately tuned (12). If the avidity is too high, the nanoparticles remain strongly associated with the endothelial cells of the BBB, whereas nanoparticles of lower avidity are able to release into the brain after transcytosis. Although the lower-avidity nanoparticles showed the greatest ability to enter the brain, the higher-avidity nanoparticles still were able to cross the BBB in greater amounts than non-Tf-containing nanoparticles.

As with Ab BBB transcytosis, the nanoparticles with reduced avidity to TfR showed the greatest ability to cross the BBB. A major obstacle to translating these agents to viable therapeutics is the need to dose very high quantities in the blood for an appreciable amount of drug to reach the CNS (6, 9, 12). We attempted to increase the ability of Tf-containing nanoparticles to reach the brain parenchyma by incorporating a small chemical linker between the Tf and AuNP cores that cleaves at mildly acidic pH. This design provides for high-avidity interactions with TfR at the blood side of the BBB to enable practical, systemic dosing amounts. Then, as the targeted nanoparticles transcytose, we use the drop in pH (13, 14) the bound nanoparticles would experience during the transcytosis process to trigger the cleavage of the linkage between the Tf and the nanoparticle core. Thus, when the transcytosing vesicle reaches the brain, the nanoparticles will no longer be bound and can be released into the parenchyma. With this design, the nanoparticle will retain high-avidity interactions with TfR on the blood side of the BBB, but not be restricted once within the endothelium (Fig. 1*A*). Recently, in vitro

Significance

Treatment for many neurological diseases is hindered by the inability of therapeutic agents to cross the blood–brain barrier (BBB). Here, we show a method for increasing the ability of high-avidity, transferrin (Tf)-containing nanoparticles to enter the brain through transcytosis. Tf was attached to nanoparticles through an acid-cleavable linkage that facilities release of nanoparticles from Tf that are bound to Tf receptors (TfR) during transcytosis, promoting entry of the nanoparticles into the brain. This method is an improvement over previous high-affinity, TfR-targeted therapeutics that were restricted by BBB endothelium and mostly excluded from entering the brain. Increased brain accumulation of nanoparticles via this methodology should allow for greater delivery of encapsulated therapeutic agents at lower systemic doses.

Author contributions: A.J.C. and M.E.D. designed research; A.J.C. performed research; A.J.C. contributed new reagents/analytic tools; A.J.C. and M.E.D. analyzed data; and A.J.C. and M.E.D. wrote the paper.

The authors declare no conflict of interest.

Freely available online through the PNAS open access option.

[1]To whom correspondence should be addressed. Email: mdavis@cheme.caltech.edu.

This article contains supporting information online at www.pnas.org/lookup/suppl/doi:10.1073/pnas.1517048112/-/DCSupplemental.

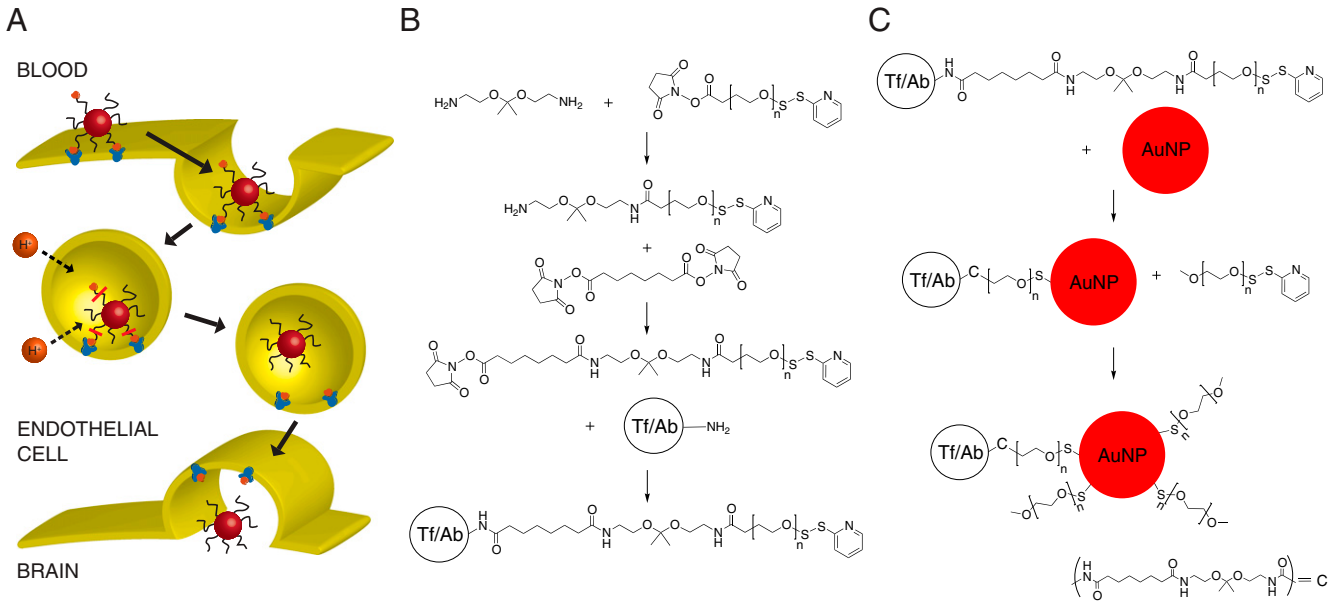

Fig. 1. (*A*) Proposed mechanism of transcytosis for Tf-containing nanoparticles with an acid-cleavable linkage. After endocytosis, rapid acidification of the endosome causes separation of the Tf ligand from the nanoparticle core, allowing free movement of the nanoparticle into the brain parenchyma once transcytosis is complete. (*B*) Preparation of acid-cleavable DSS-DAK-PEG-OPSS and addition to the targeting ligand (Tf/Ab) to create the cleavable conjugate. (*C*) Addition of the Tf/Ab-DAK-PEG-OPSS ligand followed by excess mPEG-SH to prepare targeted gold nanoparticles. n ~ 120 for 5-kDa PEG.

results using an anti-TfR Ab with reduced affinity at pH 5.5 showed the ability to transcytose across hCMEC/D3 cells, whereas Abs with high affinity independent of pH were trafficked to the lysosome (15), suggesting vesicle trafficking may be affected by a particular targeting ligand. Thus, we also investigated whether Tf, the natural ligand for the TfR, and anti-TfR Abs behaved differently when used as the targeting agents for the nanoparticles. Our results show a nearly threefold increase in the ability of high-avidity nanoparticles to reach the brain parenchyma in vivo after incorporation of an acid-cleavable, diamino ketal (DAK) linker. We also observed a direct relationship between brain penetration of nanoparticles and surface Tf-DAK content. Furthermore, no improvement was seen in the ability for anti-TfR Ab-containing nanoparticles to cross the BBB with addition of the DAK linker, suggesting there are significant differences in their intracellular trafficking compared with that of Tf-containing nanoparticles.

Results

Synthesis and Characterization of Acid-Cleavable, Ligand–PEG Conjugates. The acid-sensitive DAK [2,2-bis(aminoethoxy)propane] moiety was added to a 5-kDa polyethylene glycol (PEG), followed by conjugation of the polymer to either human holo-Tf or R17217 anti-mouse TfR Ab (Fig. 1*B* and *SI Appendix*, Fig. S1). DAK was chosen because its reported hydrolysis half-life is 60 min at pH 5.5 but more than 24 h at pH 7.4 and 37 °C (16). These hydrolysis kinetics should provide sufficient Ligand-DAK-PEG stability for the Tf/Ab to remain associated with the nanoparticle while it is circulating in the blood, but cleave in the acidic vesicles during the transcytosis process, so that the majority of the ligand disassociates from the nanoparticle core during that time. The stability of the Tf-DAK-PEG (Tf-C) conjugate was monitored by MALDI-TOF and found to release Tf within 2 h once placed in pH 5.5 buffer at 37 °C (*SI Appendix*, Fig. S2*A*). The conjugate remained virtually unchanged at pH 8 after 2 h and could still be detected after 24 h (*SI Appendix*, Fig. S2*B*).

Tf/Ab-DAK-PEG-Containing Nanoparticles Have Decreased Avidity to TfR After Exposure to Mildly Acidic pH. To prepare the targeted nanoparticles, various quantities of either cleavable (Tf-C/Ab-C) or noncleavable (Tf-N/Ab-N) ligand were added to 50-nm AuNPs, followed by an addition of excess, nonfunctionalized PEG (mPEG) (Fig. 1*C*). AuNPs were chosen for the utility of their detection within biological systems through transmission electron microscopy, inductively coupled plasma mass spectrometry (ICP-MS), or silver enhancement. Nanoparticles were prepared in this manner to preserve the characteristics we found useful in our previous formulations, which showed that ~80-nm nanoparticles with near-neutral zeta potentials (<−15 mV) best enter the brain (12). Also, sub-100-nm nanoparticles with dense PEG coating and near-neutral zeta potentials have shown the ability to diffuse throughout the brain's extracellular space (17). All nanoparticle formulations prepared here had hydrodynamic diameters near 80 nm, as measured by dynamic light scattering, and zeta potentials between −11 and −5 mV when measured in 1 mM KCl (Table 1).

An in vitro, cell-binding assay was performed using the Neuro2A mouse brain endothelial cell line to determine the avidity of the nanoparticles to mouse TfRs. Cells were incubated with

Table 1. Nanoparticle formulations and characteristics

Formulation	Nanoparticle diameter, nm	Zeta potential, mV	K_d, nM
mPEG	75.1 ± 2.4	−5.75 ± 4.12	N.D.
20Tf-N	79.1 ± 0.9	−5.77 ± 2.21	0.408
200Tf-N	78.1 ± 6.2	−7.78 ± 3.73	0.029
20Tf-C	75.7 ± 4.4	−11.25 ± 1.81	0.788
120Tf-C	77.2 ± 0.2	−7.93 ± 0.60	0.096
200Tf-C	73.6 ± 1.6	−7.47 ± 3.12	0.030
2Ab-N	76.1 ± 4.3	−6.26 ± 2.00	0.441
10Ab-N	84.4 ± 6.9	−8.83 ± 2.19	0.039
2Ab-C	72.9 ± 4.9	−6.36 ± 2.44	0.619
10Ab-C	77.4 ± 1.9	−5.10 ± 2.31	0.021

The number in the formulation name indicates the number of ligands per nanoparticle, -N indicates noncleavable PEG conjugate, and -C indicates cleavable PEG conjugate. Data shown for hydrodynamic diameter and zeta potential are the average of 5 measurements ±1 SD. N.D. = not determined.

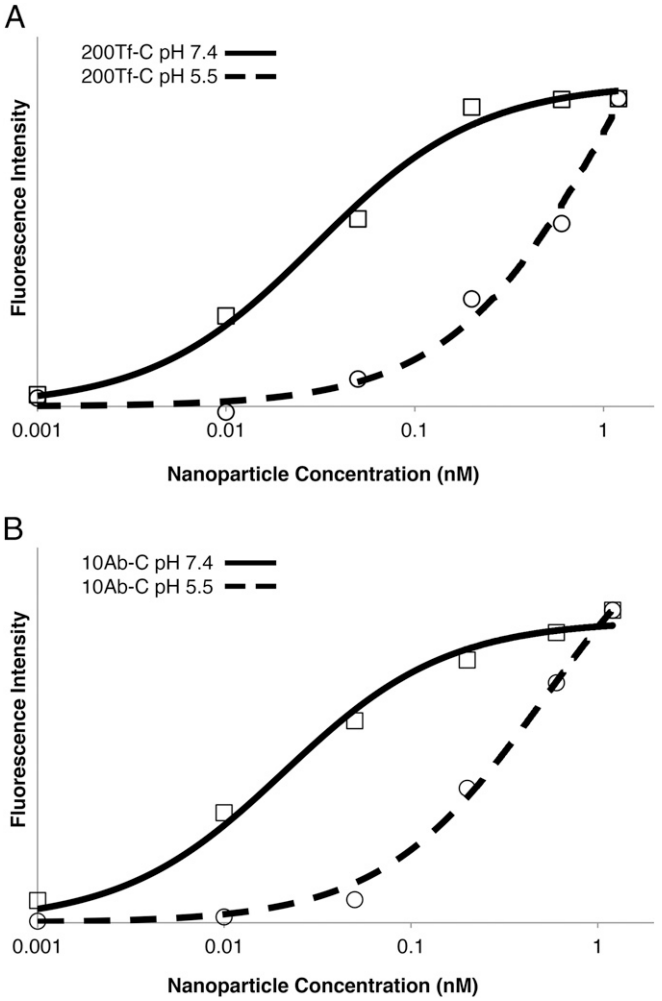

Fig. 2. Tf/Ab-DAK-PEG-containing nanoparticles have decreased avidity for mouse TfR after exposure to mildly acidic pH. (*A*) Nanoparticle binding to Neuro2A cells for 200Tf-C formulation after exposure to either neutral or acidic pH. 200Tf-C nanoparticles bind with high avidity (K_d = 0.040 nM) when kept at pH 7.4, but avidity is reduced after incubating nanoparticles at pH 5.5 (K_d = 1.16 nM). (*B*) The same effects are observed with 10Ab-C formulation (K_d = 0.021 nM at pH 7.4; K_d = 0.512 nM after pH 5.5), as in *A* with 200Tf-C. Curves are fitted Langmuir binding isotherms.

increasing quantities of nanoparticles. Then the bound nanoparticles were quantified by silver enhancement, a highly sensitive AuNP detection method (18). The binding data were fit to a Langmuir binding isotherm to calculate K_d (*SI Appendix*, Fig. S3). The binding avidity was directly dependent on the ligand content of the nanoparticle (Table 1), as we have shown previously (12). Also, by increasing the quantity of Tf contained on the nanoparticle, avidities similar to those of the nanoparticles containing the R17217 Ab with lower protein numbers could be obtained. The cell-binding assay was repeated for the 200Tf-C and 10Ab-C formulations after incubating the particles at pH 5.5 for 4 h at 37 °C. Both formulations showed lower avidity to TfR (K_d = 1.16 nM for 200Tf-C; K_d = 0.512 nM for 10Ab-C) after exposure to decreased pH, indicating loss of the surface ligand (Fig. 2).

High-Avidity Tf-DAK-PEG-Containing Nanoparticles Cross an in Vitro Model of the BBB Rapidly and in the Greatest Amounts. To assess how the addition of the DAK linker may affect the ability of the targeted nanoparticles to cross the BBB in vivo, we used the bEnd.3 cell line, an immortalized mouse brain endothelial line, in a commonly used in vitro model of the BBB (19). Nanoparticles were added to the apical compartment of bEnd.3-coated transwells in serum-free DMEM and allowed to cross the cellular border over the course of 8 h. The full volume of the basal compartment was removed and replaced by fresh, serum-free DMEM at various points. These samples were then measured for gold content using ICP-MS.

After 8 h, the 200Tf-C formulation showed the greatest capacity to cross the BBB model membrane (Fig. 3*A*). These nanoparticles reach the basal compartment at a 10-fold increased quantity compared with the 200Tf-N formulation. All Tf-containing formulations reveal decreased ability to cross the bEnd.3 cells when coincubated with serum concentrations of Tf, indicating specific binding of TfR is responsible for crossing (*SI Appendix*, Fig. S4). Unlike the high-avidity Tf-C formulations, the Ab-C formulations did not show a significant difference in basal well accumulation compared with Ab-N. In fact, all Ab-containing formulations showed similar or less crossing than nontargeted mPEG particles (*SI Appendix*, Fig. S5). After the 8-h incubation, the cells exposed to the high-avidity formulations (200Tf-N, 200Tf-C, 10Ab-N) were lysed, and intracellular gold content was measured (*SI Appendix*, Fig. S6). The 10Ab-N formulation had significantly more gold within the cells compared with 200Tf-C, consistent with high-affinity Abs being primarily retained by endothelial cells rather than transcytosing.

Interestingly, all three Tf-C formulations underwent the majority of their total crossing within the first 60 min after introduction

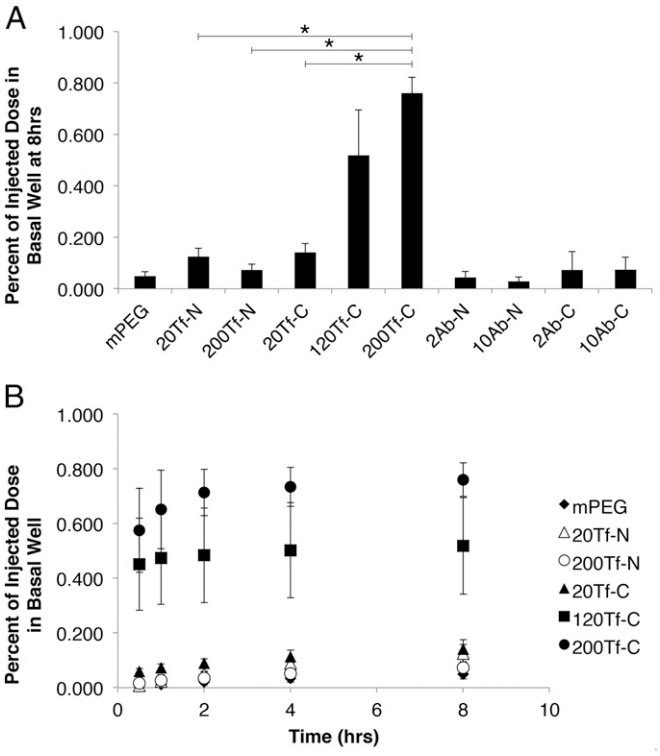

Fig. 3. 120Tf-C and 200Tf-C nanoparticles cross an in vitro model of the BBB in greater amounts than 20Tf-N and 200Tf-N. (*A*) Percentage of injected nanoparticles reaching the basal well of bEnd.3 coated transwells 8 h after introduction. 120Tf-C and 200Tf-C show greater ability to cross the transwells compared with 200Tf-N, whereas both Ab-C formulations did not show a significant increase compared with equivalent Ab-N formulations. (*B*) Tf-containing nanoparticles crossing the model BBB over time. All Tf-C formulations show the majority of crossing within the first 2 h (*SI Appendix*, Table S1). The average of three wells for each group is shown (except for 20Tf-C, n = 4). Error bars given are SE. *P < 0.001.

(Fig. 3*B*). The Tf-N formulations, conversely, showed slower basal well accumulation during the 8 h (*SI Appendix*, Table S1). For example, by 60 min, only 18% of the total 20Tf-N quantity reached the basal well compared with 61% of the total 20Tf-C. AuNPs with diameters between 50 and 100 nm have been shown to rapidly sediment within in vitro systems using an upright cell orientation (20). This causes the particle concentration at the cell surface to be higher than the rest of the solution. Because each Tf-C formulation crossed the bEnd.3 cells rapidly after introduction, these results suggest that these nanoparticles are undergoing transcytosis upon initial contact with the cells, whereas the Tf-N formulations may have a larger portion recycled back to the cell surface or retained by the cells. Also, the 120Tf-C and 200Tf-C formulations reached near maximum crossing within 2 h (93% and 94% of total, respectively) compared with 200Tf-N (47%). These data indicate that the high-avidity, cleavable nanoparticles may be saturating the transcytosis pathway within 2 h of exposure.

Addition of DAK Linkage Increases the Ability of High-Avidity, Tf-Containing Nanoparticles to Enter the Brain, but Does Not Affect Those with Anti-TfR Abs. Nanoparticles of each formulation listed in Table 1 were injected into BALB/c mice and assessed for their ability to enter the brain parenchyma. A total of three mice were used for each formulation. Nanoparticles were systemically administered by injection via the lateral tail vein and allowed to circulate for 12 h. Mice were then euthanized, and the brains resected and processed for histological examination. The locations of nanoparticles within the brain were determined using silver enhancement. Deposition of metallic silver onto gold nanoparticles allows individual nanoparticles to become visible by light microscopy. Nanoparticles present within the brain parenchyma were manually counted in 40 images per mouse. The median number of nanoparticles in the parenchyma for each group is shown in Fig. 4. As with the in vitro experiment, the 200Tf-C formulation showed the highest penetration into the brain, and a significantly higher quantity compared with 200Tf-N. Also, incorporation of the cleavable link did not increase the ability of either Ab-C formulation to enter the parenchyma. The 20Tf-C formulation did not significantly differ from 20Tf-N, but more nanoparticles localized into the brain as the surface content of Tf-DAK increased. The 120Tf-C and 200Tf-C nanoparticles entered the brain best, but did not significantly differ from one another (they have relatively similar K_d values; Table 1). Results from mPEG, 20Tf-N, and 200Tf-N are essentially the same as we reported previously, using formulations of those type (12), and indicate the good reproducibility of our methods. The 20Tf-N formulation reached the parenchyma in significantly higher amounts than 200Tf-N (*SI Appendix*, Table S2), indicating the high-avidity Tf-containing nanoparticles are retained and/or stuck to the endothelium without the presence of the cleavable linker.

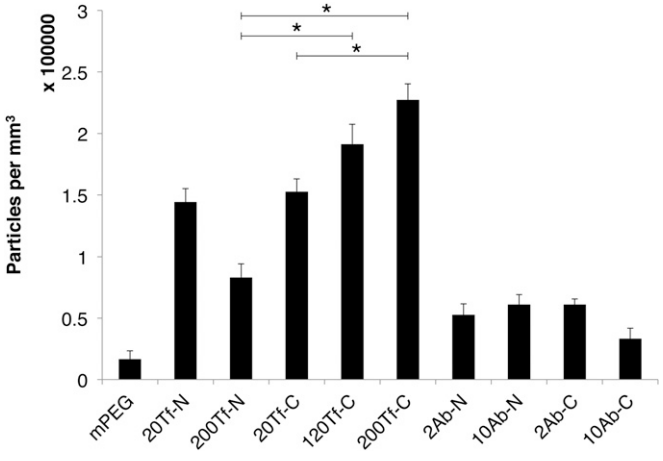

Fig. 4. Addition of DAK increases the ability of high-avidity Tf-containing nanoparticles to enter the brain in vivo. Nanoparticles within the brain parenchyma were manually counted after silver enhancement of brain sections. Three BALB/c mice were injected for each formulation. A total of 40 images per mouse brain were analyzed. Median values and SE are shown. Significant differences are displayed for select group comparisons (*$P < 0.0001$). *P* values for all potential pairwise comparisons are given in *SI Appendix*, Table S2.

Sample images for each formulation are shown in Fig. 5. Fully magnified images are available in *SI Appendix*, Figs. S8–S11. All slides were silver-stained simultaneously with a blank brain (no AuNPs injected) to assess for any nonspecific staining [some areas of nonspecific silver stain were observed in the blank sample (*SI Appendix*, Fig. S7), and similar staining patterns observed in AuNP-containing samples were not included in the analysis].

Discussion

Here, we show that high-avidity, Tf-containing nanoparticles can enter the brain in vivo in mice from systemic administrations if Tf is attached to the nanoparticle through an acid-cleavable link. This improvement over our previous design, in which high-avidity nanoparticles were restricted by the brain endothelium (12), should allow for higher brain accumulation of therapeutic agents contained in nanoparticles from a more practical, systemic dosing amount. The 20Tf-C nanoparticles did not significantly differ from the 20Tf-N, indicating that at lower avidity, the ability to outcompete endogenous Tf for TfR on the blood side of the BBB is likely the limiting factor for the processes of entering the brain. Despite the increased ability of 200Tf-C nanoparticles to enter the brain, only a 2.7-fold increase in nanoparticle accumulation was observed compared with 200Tf-N. This is likely because of the cleavage kinetics of the DAK linker. DAK was chosen because of its good stability at pH 7.4, simple incorporation into the nanoparticle design, and biologically compatible cleavage product. The trade-off, however, is slower cleavage at acidic pH. Radiolabeled-Tf has been observed in the brain parenchyma within 30 min of systemic injection (21), suggesting the length of transcytosis is on the order of tens of minutes. The Tf-DAK-PEG conjugate likely does not cleave rapidly enough during this period to dissociate all the Tf from the nanoparticle surface, causing the remaining fraction to limit entry to the brain. There is certainly room for improvement on this design, using a linkage with well-controlled cleavage kinetics. An ideal linker will cleave fully at mildly acidic pH within the timespan of transcytosis but remain stable at neutral pH long enough to allow for adequate biodistribution of the nanoparticle. Unfortunately, there is yet to be a systematic study comparing pH stability with chemical structure (22).

Unlike Tf-DAK-containing nanoparticles, both Ab-C and Ab-N formulations have a limited ability to enter the brain in vivo. These results are consistent with previous reports of high-affinity anti-TfR Abs trafficking to the lysosome (10, 11, 13). If Ab-TfR interactions dictate trafficking of the endocytic vesicle, whether the nanoparticle core is covalently attached to the ligand or a separate entity should have no effect on the transcytosis capacity. The mechanism that triggers trafficking to the lysosome, however, is unclear. Experiments with anti-TfR Abs have suggested either high-affinity (10) or multivalent binding (11) disrupts TfR processing. We did not observe the same limitations with high-avidity, multivalent Tf-containing nanoparticles, which were able to enter the brain parenchyma, albeit at reduced amounts compared with lower-avidity nanoparticles. These results suggest that the native ligand may not adversely affect intracellular sorting of the targeted therapeutic in the same way or to the same degree as with Abs. It is well established that Tf disassociates from TfR at mildly acidic pH (23). Also, the Tf–TfR

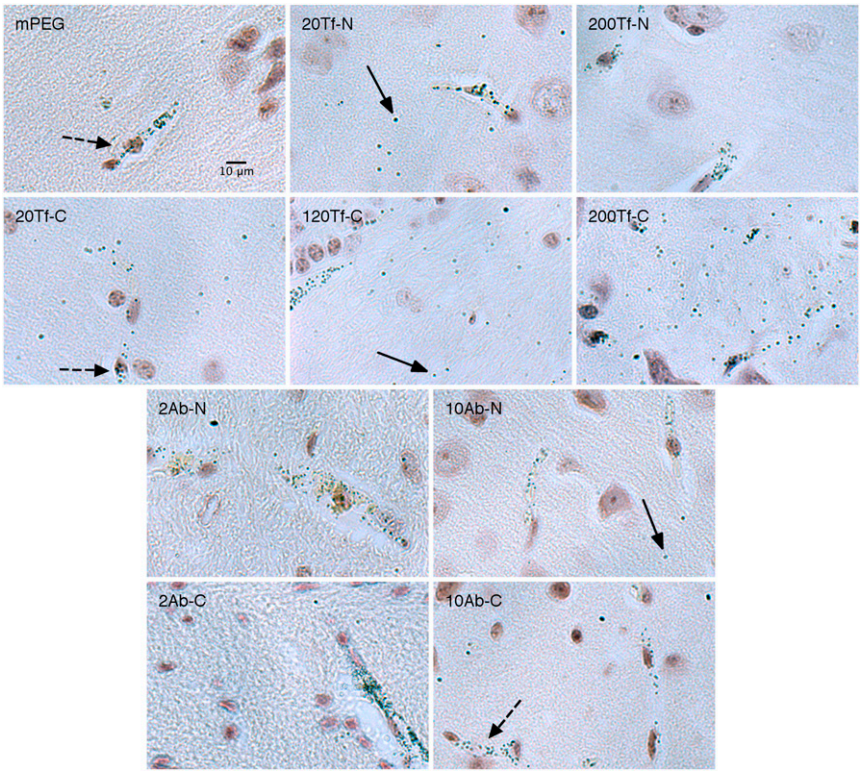

Fig. 5. Nanoparticles imaged within the brain after silver enhancement. Nanoparticles were injected i.v. into mice and allowed to circulate for 12 h. Solid arrows indicate examples of nanoparticles present in the brain parenchyma. Dashed arrows indicate examples of nanoparticles within blood vessels. The denotation of the formulation is shown in the upper left of each image. All images are to the same scale as shown in the first image at the top left.

complex is known to undergo significant conformational changes after the pH change (24). It is possible that continuous occupation of TfR by pH-independent, high-affinity Abs inhibits necessary conformational changes in the Tf–TfR complex, causing sorting to the lysosome. The cleavable nanoparticles containing Tf (e.g., 200Tf-C), however, decrease the influence of the nanoparticle core on Tf–TfR interactions by physically separating the nanoparticle from the ligand. Thus, Tf sorting may be able to occur more normally, whereas the rest of the nanoparticle remains a passenger in the transcytotic vesicle.

The ultimate goal of our work is to develop a safe method to deliver a wide spectrum of therapeutic agents to the CNS (we have already translated nanoparticles carrying small-molecule chemotherapeutics and siRNAs to the clinic). Although 200Tf-C revealed the best results here for entering the brain, the amounts achieved are still on the order of 1% of the injected dose reaching the brain parenchyma. Whether this quantity is sufficient to deliver enough therapeutic and/or imaging agent to the brain for practical use is currently under investigation. As we mentioned previously, we believe that faster release kinetics could be advantageous to increasing the amounts that reach the brain. Other chemical linkers that are sensitive to endosomal changes, such as disulfides, may also benefit from this cleavable ligand strategy, provided they break rapidly enough during transcytosis.

Here, we show that high-avidity, Tf-containing nanoparticles are capable of entering the brain parenchyma when Tf is bound to the nanoparticle through an acid-cleavable link. Exposure to the decreased pH during the transcytosis process causes the nanoparticle core to separate from surface Tf bound to TfR and increases the nanoparticle's ability to enter the brain parenchyma. In contrast, nanoparticles containing anti-TfR Abs were essentially excluded from the brain independent of the cleavable link, likely by their trafficking to lysosomes. All Tf-containing formulations with or without the cleavable link showed a greater ability to enter the brain than any Ab-containing ones. These results suggest that TfR-targeted therapeutics using the native ligand, rather than a high-affinity Ab, may have a greater ability to cross the BBB. Our results suggest that better understanding of TfR trafficking within the brain endothelium on a ligand-by-ligand basis is necessary to develop therapeutics that can readily engage and be successful in the TfR-mediated transcytosis process at the BBB.

Materials and Methods

Complete details of the materials and methods used in this study are provided in *SI Appendix*.

DSS-DAK-PEG-OPSS Synthesis. N-hydroxysuccinimide-PEG-orthopyridyl disulfide (NHS-PEG-OPSS) was reacted with DAK to prepare DAK-PEG-OPSS. Unreacted NHS-PEG-OPSS was quenched by addition of *N*-(2-aminoethyl)aminomethyl polystyrene beads for 1 h. Disuccinimidyl suberate (DSS) was added to DAK-PEG-OPSS to prepare DSS-DAK-PEG-OPSS.

Preparation of Ligand-DAK-PEG-OPSS. Ligand (either Tf or Ab) was added to DSS-DAK-PEG-OPSS to prepare Ligand-DAK-PEG-OPSS (*SI Appendix*, Fig. S1 *B* and *D*). High-order PEGylated species were removed by hydrophobic interaction chromatography (HIC) to yield a mixture of unreacted ligand and mono-PEGylated ligand. The amount of ligand-DAK-PEG-OPSS in the mixture was determined by quantifying OPSS present. The Tf-containing conjugate was reloaded with iron after HIC by incubating with iron citrate.

Estimation of Ligand-DAK-PEG Stability at pH 5.5. Tf-DAK-PEG was added to 100 mM sodium acetate buffer pH 5.5, 37 °C. At various points, aliquots were removed, diluted in pH 8 buffer, and frozen on CO_2(s) until analysis. Samples were thawed simultaneously and run on MALDI-TOF, using a sinapinic acid matrix to determine protein conjugate stability.

Preparation of Ligand-PEG-OPSS. Ligand (either Tf or Ab) was added to NHS-PEG-OPSS to form ligand-PEG-OPSS (*SI Appendix*, Fig. S1 *A* and *C*). Tf-PEG-OPSS was separated by HPLC followed by HIC to yield a pure, mono-PEGylated fraction, whereas Ab-PEG-OPSS was purified using only HIC. The Tf-containing conjugate was reloaded with iron, as described previously.

Preparation of Targeted Nanoparticles. Noncleavable or acid-cleavable Ligand-PEG conjugates were added to 50-nm AuNPs at the appropriate molar excess (e.g., 20× mol excess Tf-PEG for 20Tf per particle) for 60 min. An excess quantity of mPEG-SH was then added for a further 30 min. AuNP's were pelleted by centrifugation, resuspended in water, and sonicated for 5 min. The washing procedure was performed a total of three times.

Dynamic Light Scattering. Particle sizes and zeta potentials were measured with a Brookhaven Instruments ZetaPALS. Values shown are from an average of five runs for nanoparticle size and five runs with a target residual of 0.02 for zeta potential.

Nanoparticle Cell-Binding Assay. Increasing quantities of nanoparticles were added to fixed Neuro2A cells after exposure to either pH 7.4 or pH 5.5 buffer. The particles were allowed to bind for 90 min, with light mixing every 15 min to avoid settling. Cells were then washed in PBS three times to remove unbound nanoparticle and treated with silver enhancement. Bound gold content was measured by fluorescence in a 96-well plate reader (Tecan Infinite M200; excitation, 310 nm; emission, 400 nm). The data were fit to a Langmuir binding isotherm, with B_{max} and K_d determined using MATLAB (Mathworks).

Nanoparticle Transwell Assay. bEnd.3 cells were grown on polyester membrane transwells (Corning) until transendothelial electrical resistance (TEER) was more than 30 Ohm*cm^2. A total of 1×10^{10} AuNPs were added to the apical compartment in serum-free DMEM. The entire basal well volume was removed at various points and replaced with fresh media. An Agilent HP 7500 ICP-MS was used to measure the gold content of the basal well aliquots.

In Vivo Analysis. All animals were treated according to the NIH guidelines for animal care and use (25) as approved by the Caltech Institutional Animal Care and Use Committee. Female BALB/c mice (The Jackson Laboratory) were injected with 4.5×10^{11} particles via lateral tail vein. After 12 h, the mice were euthanized by CO_2 asphyxiation and their brains were resected, bisected, and fixed in 10% formalin. The brain hemispheres were then embedded in paraffin, sectioned, deparaffinized, and treated with silver enhancement (Ted Pella). Sections were counterstained with hematoxylin, mounted, and imaged using an Olympus IX50 microscope with a 40× objective. Ten images were acquired randomly from rostral, ventral, and dorsal regions and the cerebellum to give 40 total images per brain. Nanoparticles within the brain parenchyma were manually counted. Image acquisition and particle counting was performed blindly for all slides. Statistical significance for pairwise group comparisons was tested using the Wilcoxon rank-sum test.

ACKNOWLEDGMENTS. We thank Nathan Dalleska (Caltech Environmental Analysis Center) for his assistance with ICP-MS measurements and Mona Shahgohli (Caltech) for assistance with MALDI-TOF measurements. This work was supported by National Institutes of Health Grant R01 NS0711121 and National Cancer Institute Grant CA 151819.

1. Pardridge WM (2005) The blood-brain barrier: Bottleneck in brain drug development. *NeuroRx* 2(1):3–14.
2. Chen Y, Liu L (2012) Modern methods for delivery of drugs across the blood-brain barrier. *Adv Drug Deliv Rev* 64(7):640–665.
3. Jones AR, Shusta EV (2007) Blood-brain barrier transport of therapeutics via receptor-mediation. *Pharm Res* 24(9):1759–1771.
4. Kinoshita M, McDannold N, Jolesz FA, Hynynen K (2006) Noninvasive localized delivery of Herceptin to the mouse brain by MRI-guided focused ultrasound-induced blood-brain barrier disruption. *Proc Natl Acad Sci USA* 103(31):11719–11723.
5. Uchida Y, et al. (2011) Quantitative targeted absolute proteomics of human blood-brain barrier transporters and receptors. *J Neurochem* 117(2):333–345.
6. Lajoie JM, Shusta EV (2015) Targeting receptor-mediated transport for delivery of biologics across the blood-brain barrier. *Annu Rev Pharmacol Toxicol* 55(1):613–631.
7. Widera A, Norouziyan F, Shen WC (2003) Mechanisms of TfR-mediated transcytosis and sorting in epithelial cells and applications toward drug delivery. *Adv Drug Deliv Rev* 55(11):1439–1466.
8. Friden PM, et al. (1991) Anti-transferrin receptor antibody and antibody-drug conjugates cross the blood-brain barrier. *Proc Natl Acad Sci USA* 88(11):4771–4775.
9. Yu YJ, et al. (2011) Boosting brain uptake of a therapeutic antibody by reducing its affinity for a transcytosis target. *Sci Transl Med* 3(84):84ra44.
10. Bien-Ly N, et al. (2014) Transferrin receptor (TfR) trafficking determines brain uptake of TfR antibody affinity variants. *J Exp Med* 211(2):233–244.
11. Niewoehner J, et al. (2014) Increased brain penetration and potency of a therapeutic antibody using a monovalent molecular shuttle. *Neuron* 81(1):49–60.
12. Wiley DT, Webster P, Gale A, Davis ME (2013) Transcytosis and brain uptake of transferrin-containing nanoparticles by tuning avidity to transferrin receptor. *Proc Natl Acad Sci USA* 110(21):8662–8667.
13. Mellman I (1996) Endocytosis and molecular sorting. *Annu Rev Cell Dev Biol* 12:575–625.
14. Mellman I, Fuchs R, Helenius A (1986) Acidification of the endocytic and exocytic pathways. *Annu Rev Biochem* 55:663–700.
15. Sade H, et al. (2014) A human blood-brain barrier transcytosis assay reveals antibody transcytosis influenced by pH-dependent receptor binding. *PLoS One* 9(4):e96340.
16. Binauld S, Stenzel MH (2013) Acid-degradable polymers for drug delivery: A decade of innovation. *Chem Commun (Camb)* 49(21):2082–2102.
17. Nance EA, et al. (2012) A dense poly(ethylene glycol) coating improves penetration of large polymeric nanoparticles within brain tissue. *Sci Transl Med* 4(149):149ra119.
18. Cao X, Ye Y, Liu S (2011) Gold nanoparticle-based signal amplification for biosensing. *Anal Biochem* 417(1):1–16.
19. Brown RC, Morris AP, O'Neil RG (2007) Tight junction protein expression and barrier properties of immortalized mouse brain microvessel endothelial cells. *Brain Res* 1130(1):17–30.
20. Cho EC, Zhang Q, Xia Y (2011) The effect of sedimentation and diffusion on cellular uptake of gold nanoparticles. *Nat Nanotechnol* 6(6):385–391.
21. Fishman JB, Rubin JB, Handrahan JV, Connor JR, Fine RE (1987) Receptor-mediated transcytosis of transferrin across the blood-brain barrier. *J Neurosci Res* 18(2):299–304.
22. Leriche G, Chisholm L, Wagner A (2012) Cleavable linkers in chemical biology. *Bioorg Med Chem* 20(2):571–582.
23. Dautry-Varsat A, Ciechanover A, Lodish HF (1983) pH and the recycling of transferrin during receptor-mediated endocytosis. *Proc Natl Acad Sci USA* 80(8):2258–2262.
24. Luck AN, Mason AB (2013) Structure and dynamics of drug carriers and their interaction with cellular receptors: Focus on serum transferrin. *Adv Drug Deliv Rev* 65(8):1012–1019.
25. Committee on Care and Use of Laboratory Animals (1996) *Guide for the Care and Use of Laboratory Animals* (Natl Inst Health, Bethesda), DHHS Publ No (NIH) 85–23.